

A Nearly Information Theoretically Secure Approach for Semantic Communications over Wiretap Channel

Weixuan Chen, *Graduate Student Member, IEEE*, Shuo Shao, Qianqian Yang, *Member, IEEE*, Zhaoyang Zhang, *Senior Member, IEEE*, Ping Zhang, *Fellow, IEEE*

Abstract—This paper addresses the challenge of achieving information-theoretic security in semantic communication (SeCom) over a wiretap channel, where a legitimate receiver coexists with an eavesdropper experiencing a poorer channel condition. Despite previous efforts to secure SeCom against eavesdroppers, achieving information-theoretic security in such schemes remains an open issue. In this work, we propose a secure digital SeCom approach based on superposition codes, aiming to attain nearly information-theoretic security. Our proposed method involves associating semantic information with satellite constellation points within a double-layered constellation map, where cloud center constellation points are randomly selected. By carefully allocating power between these two layers of constellation, we ensure that the symbol error probability (SEP) of the eavesdropper decoding satellite constellation points is nearly equivalent to random guessing, while maintaining a low SEP for the legitimate receiver to successfully decode the semantic information. Simulation results showcase that the Peak Signal-to-Noise Ratio (PSNR) and Mean Squared Error (MSE) for the eavesdropper’s reconstructed data, using our proposed method, can range from decoding Gaussian-distributed random noise to approaching the variance of the data. This validates the ability of our method to achieve nearly information-theoretic security, demonstrating superior data security compared to benchmark methods.

Index Terms—Digital semantic communications, superposition code, wiretap channel, information-theoretic security.

I. INTRODUCTION

Semantic communication (SeCom) [1] [2], emerging as a novel communication paradigm, has received significant attention in recent years due to its capability to facilitate efficient transmission for data-intensive applications. This innovative approach focuses on extraction and transmission of essential information, referred to as *semantic information* [3], crucial for data reconstruction or task execution, while discarding irrelevant details. Consequently, SeCom stands out as a bandwidth-efficient communication paradigm that enhances the transmission efficiency of communication systems and improves the quality of intelligent information services. Deep learning (DL) techniques, proven highly effective in various domains [4] [5] [6], play a pivotal role in SeCom systems by leveraging neural networks (NNs) to perform joint source and channel coding (Deep JSCC) [7] on the source data. This integration of DL enables SeCom systems to achieve excellent performance in transmitting various types of information, such as text [8] [9], speech [10] [11], image [12] [13] [14], video [15], and multimodal data [16].

The progress in SeCom also raises concerns regarding security and privacy [17] [18]. Erdemir et al. [19] proposed a secure SeCom system designed for wiretap channels. This approach utilized a variational autoencoder (VAE)-based NN architecture and incorporated a specially designed loss function for end-to-end training, striking a balance between minimizing information leakage to potential eavesdropper and maintaining low distortion at the legitimate receiver. In a related work, Marchioro et al. [20] developed a data-driven secure SeCom scheme leveraging a generative adversarial training method by treating the eavesdropper as an adversary and penalizing the information leakage. Note that both works assume knowledge of the eavesdropper’s network to assist in training the legitimate user’s network. Specifically, it is assumed that the legitimate user can minimize the correlation between the eavesdropper’s output and the classification label to prevent information leakage. However, this assumption may be impractical in real-world scenarios. Moreover, treating information leakage as a penalty in the training process lacks a theoretical guarantee for the security of the SeCom systems.

Different from the aforementioned schemes, Tung et al. [21] utilized a conventional public key cryptographic scheme proposed in [22] to encrypt the signals to be transmitted, thus protecting the proposed deep JSCC scheme for wireless image transmission against eavesdroppers. Notably, this approach alleviates the assumption of knowing the eavesdropper’s model. However, it still falls short of ensuring the security of SeCom systems due to its vulnerability to quantum computing attacks [23] [24] and traditional attack methods, including related-key attacks [25]. Furthermore, similar to the aforementioned works, it focuses on analog SeCom systems, posing challenges for deployment in the current wireless communication systems.

To address these challenges, this paper explores an information-theoretically secure approach for DL-based digital SeCom systems considering wiretap channel [26] with additive Gaussian white noise (AWGN). Similarly, the considered system consists of a transmitter referred to as *Alice*, a legitimate receiver called *Bob*, and an eavesdropper called *Eve*. Alice aims to transmit the semantic information extracted from source data \mathbf{X} to Bob over an AWGN channel. However, Eve can wiretap the transmitted data and attempt to reconstruct the source data over another AWGN channel with worse channel condition, i.e., larger noise. The goal of this paper is to minimize the distortion of reconstructing \mathbf{X} at the receiver end

while simultaneously ensuring a theoretical guarantee against information leakage to Eve.

However, developing a theoretically secure approach for DL-based SeCom systems faces two main challenges. The signals sent by Alice contain semantically significant information extracted by NN-based encoders for the purpose of source reconstruction. This information can be captured by Eve over wiretap channel, enabling partial recovery of the source data. Additionally, traditional capacity-achieving coding schemes for Gaussian wiretap channel [27] utilizes a superposition code with two layers, employing a codebook derived through a complex two-step random codebook generation process. The intricate nature of this process makes it difficult for NN-based encoders to learn.

Inspired by the traditional coding scheme, we propose a superposition code based secure digital SeCom approach, involving three main steps. Firstly, we impose two constellation maps in digital modulation [28] to implement the superposition code. For instance, by overlaying the constellation map of 4-QAM modulation onto another 4-QAM constellation map, we create a 16-QAM constellation map. The symbol sequence of the inner constellation map is considered the cloud center codeword of the superposition code, while that of the outer constellation map is the satellite codeword. Secondly, we modulate the extracted semantic information onto the outer constellation map and randomly generate symbols for the inner constellation map. This randomly generated inner constellation point is inspired by the classic coding scheme in the wiretap channel and serves as a random key for encrypting the semantic information. Last, we dynamically adjust the power allocation between the inner and outer constellation maps based on the symbol error probability (SEP) of both the legitimate receiver and the eavesdropper. The optimal power allocation is determined by minimizing the SEP of the legitimate receiver while maintaining a constraint on the SEP of the eavesdropper. The numerical results confirm the information-theoretically guaranteed security of the proposed approach, even when dealing with high compression ratios.

The rest of the paper is structured as follows. Section II provides a brief overview of related work in our study. Section III outlines our problem setup and system design. Section IV details our constellation map design and the power allocation scheme. Section V covers the experimental setup and performance evaluation. Lastly, Section VI concludes the paper.

Notation: $\mathbb{R}^{n \times m}$ represent set of real matrices of size $n \times m$. $\|\cdot\|_2$ denotes the l_2 -norm of a given variable. $\mathbf{x} \sim \mathcal{CN}(\mu, \sigma^2)$ / $\mathbf{x} \sim \mathcal{N}(\mu, \sigma^2)$ means variable \mathbf{x} follows a circularly-symmetric complex Gaussian distribution / Gaussian distribution with mean μ and variance σ^2 .

II. RELATED WORKS

In this section, we review the related works on security and privacy protection aspects of SeCom. The identified challenges in ensuring security and privacy in SeCom are as follows. Despite the success of SeCom and deep JSCC, deep JSCC is vulnerable to eavesdropping attacks because it directly maps

the source data to the channel input symbols, resulting in an inherent correlation between the channel input symbols and the source data. Another significant challenge arises from the potential tampering of the shared semantic knowledge base by malicious entities. In such cases, the receiver encounters difficulties in accurately recovering the source data. Additionally, the sharing of a semantic knowledge base introduces concerns regarding privacy leakage. Further, attackers can send malicious semantic data with similar semantic information but different target content, causing the receiver to recover incorrect source data or make erroneous decisions.

Regarding security of SeCom systems, Sagduyu et al. [29] delved into the multi-domain security challenges associated SeCom. Employing adversarial learning, they introduced subtle perturbations to input images, disrupting the semantic decoder's input at the receiver. Through a multi-domain attack, they altered the semantics of transmitted information in the SeCom system, highlighting the risks posed by multi-domain adversarial attacks on semantic delivery and emphasizing the necessity for defense mechanisms. Du et al. [30] investigated wireless communication security in Semantic Internet-of-Things (SIoT) and proposed novel security performance indicators applied to SIoT, with a focus on semantic information transmission. From the perspective of semantic information security, they analyzed and compared some classical security techniques and reviewed some attack methods and defense methods. Lin et al. [31] proposed a blockchain-aided secure SeCom framework. Through adversarial training, the system gained the ability to distinguish adversarial semantic data from authentic data, thereby preventing semantic attacks resulting from data mutations. In a comprehensive overview, Yang et al. [32] explored various security techniques in SeCom, encompassing information bottleneck security, covert SeCom, and physical layer security. Furthermore, they scrutinized the vulnerabilities of semantic machine learning, identified known threats, and proposed potential countermeasures against them.

Regarding the privacy protection of SeCom, Luo et al. [33] introduced an encrypted SeCom system addressing the privacy leakage risk associated with sharing background knowledge. The proposed system shares its training database and ensures privacy protection through key encryption. Notably, they devised an adversarial encryption training scheme to maintain the system's transmission performance with or without encryption. Zhao et al. [34] proposed a SeCom framework combining online inference with offline training. The proposed distributed learning strategy for codec training makes it computationally impossible for attackers to implement gradient leakage attacks. Additionally, they leveraged modality-aware semantic associations to achieve personalized codec deployment, striking an effective balance between privacy protection and data utilization in SeCom. Wang et al. [35] presented a privacy protection scheme for SeCom systems using Simultaneous Transmitting and Reflecting Reconfigurable Intelligent Surface (STAR-RIS). Utilizing STAR-RIS enhanced signal transmission between the base station and the user, converting the transmitted signal into interference against eavesdroppers. This approach significantly diminished the eavesdropper's classification accuracy in image classification tasks within SeCom.

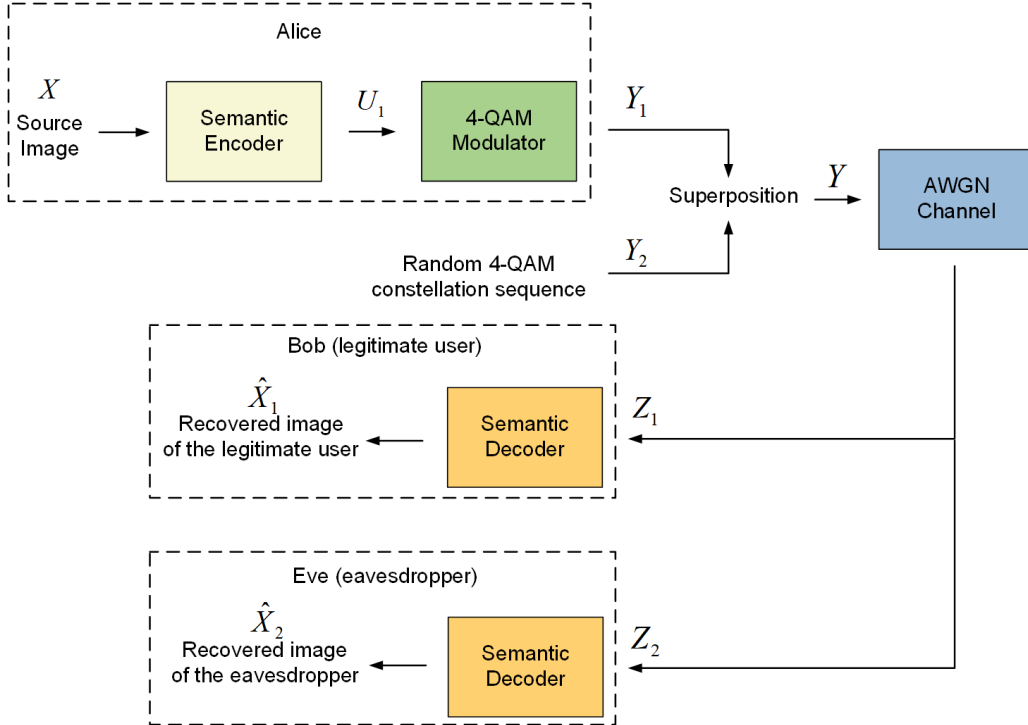


Fig. 1: The framework of the proposed secure digital SeCom system.

In another initiative, Wang et al. [36] proposed a privacy protection scheme for SeCom grounded in the information bottleneck theory and adversarial learning to defend against model inversion attacks. They extracted semantic information from the source data based on the information bottleneck metric, which is estimated by a variational upper bound on the mutual information. Additionally, they introduced an adversarial training strategy preserving privacy by minimizing the attacker's reconstruction performance.

III. PROBLEM SETUP AND SYSTEM DESIGN

A. Problem Setup

We consider a digital SeCom system for wireless image transmission over a wiretap channel with AWGN. In this system, a transmitter wants to reliably transmit a source image to a receiver. There also exists an eavesdropper attempting to recover the source image by capturing the noisy transmitted symbols. Fig. 1 shows the framework of our proposed secure digital SeCom system.

We denote the source image to transmit by \mathbf{X} , the legitimate sender by Alice, the legitimate receiver (also called the legitimate user in this paper) by Bob, and the eavesdropper by Eve, as shown in Fig. 1. Alice uses a semantic encoder to extract the semantic information \mathbf{U}_1 from \mathbf{X} , denoted by

$$\mathbf{U}_1 = f_{\text{se}}(\mathbf{X}; \boldsymbol{\theta}^{\text{se}}), \quad (1)$$

where f_{se} represents the NN-based semantic encoder, and $\boldsymbol{\theta}^{\text{se}}$ refers to the learnable parameters of f_{se} .

Semantic information \mathbf{U}_1 is then input into a NN-based 4-QAM modulator to generate the outer constellation sequence \mathbf{Y}_1 , denoted by

$$\mathbf{Y}_1 = f_{\text{mod}}(\mathbf{U}_1; \boldsymbol{\theta}^{\text{mod}}), \quad (2)$$

where f_{mod} represents the 4-QAM modulator, and $\boldsymbol{\theta}^{\text{mod}}$ refers to the learnable parameters of f_{mod} . We then randomly generate another 4-QAM constellation sequence with the same length as \mathbf{Y}_1 as the inner constellation sequence \mathbf{Y}_2 . We note that \mathbf{Y}_2 does not carry any valid information. Here, we consider 4-QAM modulation for both the outer and inner constellation for simplicity. However, we note that it can be easily extended to other modulation schemes.

We then scale and combine these two 4-QAM constellation sequences to form a 16-QAM constellation sequence \mathbf{Y} , which is transmitted over a wiretap channel with AWGN. The superposition operation is controlled by a power allocation coefficient a , denoted by

$$\mathbf{Y} = \sqrt{a} \cdot \mathbf{Y}_1 + \sqrt{1-a} \cdot \mathbf{Y}_2. \quad (3)$$

\mathbf{Y} is transmitted over the AWGN channel to Bob, who receives a noisy constellation sequence

$$\mathbf{Z}_1 = \mathbf{Y} + \mathbf{n}_1, \quad (4)$$

where $\mathbf{n}_1 \sim \mathcal{CN}(0, \sigma_1^2)$ denotes the independent and identically distributed complex Gaussian noise with a mean of 0 and a variance of σ_1^2 . Eve eavesdrops through her own AWGN channel and receives another noisy constellation sequence

$$\mathbf{Z}_2 = \mathbf{Y} + \mathbf{n}_2, \quad (5)$$

where $\mathbf{n}_2 \sim \mathcal{CN}(0, \sigma_2^2)$. Since the channel signal-to-noise ratio (SNR) of the legitimate user is usually higher than that of the eavesdropper's receiver, we assume $\sigma_1 < \sigma_2$. The channel SNR between Alice and the legitimate user is given by

$$\text{SNR}_{\text{leg}} = 10 \log_{10} \left(\frac{P}{\sigma_1^2} \right) \text{ (dB)}, \quad (6)$$

and the channel SNR between Alice and the eavesdropper by

$$\text{SNR}_{\text{eve}} = 10 \log_{10} \left(\frac{P}{\sigma_2^2} \right) \text{ (dB)}. \quad (7)$$

Both Bob and Eve share the common objective of recovering the source image. Their primary goal is to decode the outer constellation sequence, as the inner constellation sequence contains no valid information. Therefore, before being fed into the semantic decoder, both Bob and Eve try to recover the outer constellation sequence from \mathbf{Z}_1 and \mathbf{Z}_2 . Specifically, denote the coordinates of a received constellation point by (x, y) , we have

$$(\bar{x}, \bar{y}) = \begin{cases} \left(x - \sqrt{\frac{1-a}{2}}, y - \sqrt{\frac{1-a}{2}} \right), & x \geq 0, y \geq 0. \\ \left(x + \sqrt{\frac{1-a}{2}}, y - \sqrt{\frac{1-a}{2}} \right), & x < 0, y \geq 0. \\ \left(x - \sqrt{\frac{1-a}{2}}, y + \sqrt{\frac{1-a}{2}} \right), & x \geq 0, y < 0. \\ \left(x + \sqrt{\frac{1-a}{2}}, y + \sqrt{\frac{1-a}{2}} \right), & x < 0, y < 0. \end{cases}, \quad (8)$$

where (\bar{x}, \bar{y}) is the recovered outer constellation point from (x, y) . Applying this to every point in \mathbf{Z}_1 and \mathbf{Z}_2 , we then obtain the recovered outer constellation sequences at Bob and Eve, denoted by $\bar{\mathbf{Z}}_1$ and $\bar{\mathbf{Z}}_2$.

For the legitimate user, its semantic decoder performs image recovery based on $\bar{\mathbf{Z}}_1$, denoted by

$$\hat{\mathbf{X}}_1 = f_{\text{sd}}(\bar{\mathbf{Z}}_1; \boldsymbol{\theta}_1^{\text{sd}}), \quad (9)$$

where $\hat{\mathbf{X}}_1$ represents the recovered image by the legitimate user, and f_{sd} represents the semantic decoder of the legitimate user. Similarly, for the eavesdropper, we have

$$\hat{\mathbf{X}}_2 = g_{\text{sd}}(\bar{\mathbf{Z}}_2; \boldsymbol{\theta}_2^{\text{sd}}), \quad (10)$$

where $\hat{\mathbf{X}}_2$ represents the recovered image by the eavesdropper, and g_{sd} represents the semantic decoder of the eavesdropper.

B. Proposed SeCom System

Our system can be divided into five parts, including semantic encoder, 4-QAM modulator, inner constellation sequence generation, superposition constellation map design, and semantic decoder. The semantic encoder extracts the semantic information, which is then modulated by the 4-QAM modulator into the outer constellation sequence. The inner constellation sequence is generated randomly. Then we generate a superposition constellation sequence combining outer and inner constellation sequences in order to prevent information leakage to the eavesdropper. This part will be discussed in detail in section III. The semantic decoder at the receiver decodes the received signals to generate the recovered image. We describe each part of our system in detail in the following.

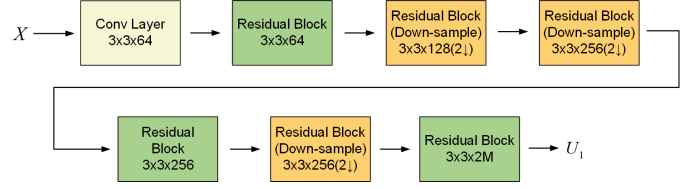


Fig. 2: The structure of the semantic encoder.

1) *Semantic Encoder and 4-QAM Modulator*: The network structure of the semantic encoder is shown in Fig. 2. The semantic encoder is used to extract information from the source image $\mathbf{X} \in \mathbb{R}^{H \times W \times 3}$ that is relevant to the image recovery task, i.e., the semantic information \mathbf{U}_1 . Here H and W are the height and width of the source image \mathbf{X} , respectively. The last dimension of \mathbf{X} corresponds to the RGB channels. The semantic encoder consists of one convolutional layer and six residual blocks as shown in Fig. 2. The number $S_{\text{kernel}} \times S_{\text{kernel}} \times C_{\text{out}}$ below each convolutional layer or residual block represents its configuration, where C_{out} is the number of output channels, and S_{kernel} is the kernel size. We note that for the residual block, S_{kernel} is the kernel size of the convolutional layer on the main path. $2 \downarrow$ means down-sampling with a stride of 2. These residual blocks perform feature extraction and down-sampling of the source image \mathbf{X} such that $\mathbf{U}_1 \in \mathbb{R}^{\frac{H}{8} \times \frac{W}{8} \times 2M}$, where M is a variable that controls the length of \mathbf{U}_1 .

The structure of the residual block with and without down-sampling is shown in Fig. 3 and Fig. 4, respectively. If the

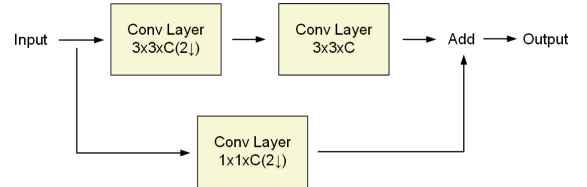


Fig. 3: The structure of the residual block with down-sampling.

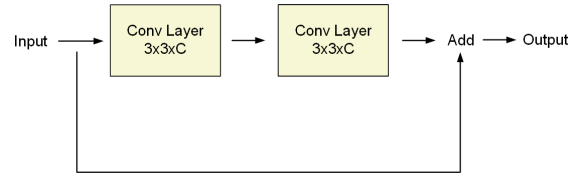


Fig. 4: The structure of the residual block without down-sampling.

residual block is of the down-sampling type, the input feature maps pass through two convolutional layers and one convolutional layer respectively. Otherwise, the separate convolutional layer is replaced by shortcut connection. The outputs of these two paths are then added together to form the output of a residual block.

Since our system is a digital SeCom system, to avoid the non-differentiability problem of directly modulating \mathbf{U}_1 , we

employ the NN-based probabilistic modulator proposed in [28] and a differentiable sampling technique. These two parts make up our 4-QAM modulator, and the network structure is shown in Fig. 5. In the proposed 4-QAM modulator,



Fig. 5: The structure of the 4-QAM modulator.

$\mathbf{U}_1 \in \mathbb{R}^{\frac{H}{8} \times \frac{W}{8} \times 2M}$ is first vectorized to $\bar{\mathbf{U}}_1 \in \mathbb{R}^{\frac{1}{32}MHW \times 1}$. Then, a NN-based probabilistic modulator, consisting of one fully connected layer, maps $\bar{\mathbf{U}}_1$ into a sequence of probability distributions $(p^{i1}, p^{i2}, p^{i3}, p^{i4})$ with each element corresponding to the probability of choosing the constellation symbols $(1 + 1j, 1 - 1j, -1 + 1j, -1 - 1j)$, respectively, where $i = 1, \dots, M$. Here $\frac{1}{32}MHW \times 4M$ below the fully connected layer represents its configuration, where $\frac{1}{32}MHW$ is the number of input neurons, and $4M$ is the number of output neurons. Then, based on this probability distribution, the constellation symbols are sampled using Gumbel-softmax method [38], which prevents the non-differentiability problem during sampling. Following this process, we modulate the semantic information \mathbf{U}_1 into a 4-QAM constellation sequence $\mathbf{Y}_1 \in \mathbb{R}^{M \times 1}$, serving as our outer constellation sequence.

2) *The Inner Constellation Sequence:* The inner constellation sequence, denoted as $\mathbf{Y}_2 \in \mathbb{R}^{M \times 1}$, is generated randomly. For each symbol within the inner constellation sequence, we select a constellation symbol from the set $(1 + 1j, 1 - 1j, -1 + 1j, -1 - 1j)$ with equal probability. The length of \mathbf{Y}_2 matches that of \mathbf{Y}_1 . The design details of the superposition constellation map will be delineated in Section III.

3) *Semantic Decoder:* We assume that the eavesdropper copies the network structure of the semantic decoder of the legitimate user to use as her own in order to steal the source image. Therefore, the structure of the semantic decoder of the eavesdropper is the same with that of the legitimate user. The semantic decoder generates the recovered image $\hat{\mathbf{X}}$ based on the received semantic information $\bar{\mathbf{Z}}$. The network structure of the semantic decoder is shown in Fig. 6, which consists

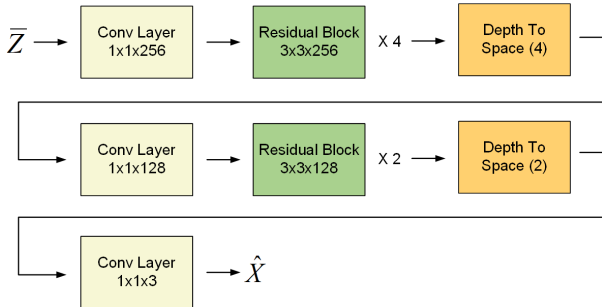


Fig. 6: The structure of the semantic decoder.

of three convolutional layers, six residual blocks and two *depth to space* modules. The *depth to space* module performs up-sampling, allowing the semantic decoder to recover the

source image. The number shown in *depth to space* box represents its configuration. If it is q , the number of the feature maps is reduced by a factor of 2^q and the height and width of the feature maps are increased by a factor of q . The output of the semantic decoder is the recovered source image $\hat{\mathbf{X}} \in \mathbb{R}^{H \times W \times 3}$.

C. Training Strategy

We introduce a two-stage training strategy to train our proposed secure digital SeCom system in this section. Unlike other studies, we do not consider preventing the eavesdropper from being able to recover the source data as an optimization goal during the training of the legitimate encoder-decoder pair (the legitimate network), due to the fact that the eavesdropper usually does not cooperate with the legitimate user during the training phase.

In the first training stage, we train only the legitimate semantic encoder-decoder pair, including the 4-QAM modulator. The loss function of the first training stage can be written as

$$\mathcal{L}_1 = MSE(\mathbf{X}, \hat{\mathbf{X}}_1), \quad (11)$$

where MSE is the mean square error (MSE) function which measures the quality of the recovered image. Note that we do not consider the eavesdropper's network in this stage.

In the second training stage, we train only the semantic decoder of the eavesdropper. We assume that the training data that the eavesdropper has are the noisy transmitted signal \mathbf{Y}_2 and the ground truth \mathbf{X} . This is the strongest setting for the eavesdropper. The loss function of the second training stage is

$$\mathcal{L}_2 = MSE(\mathbf{X}, \hat{\mathbf{X}}_2), \quad (12)$$

in order for the eavesdropper to optimize its semantic encoder.

IV. CONSTELLATION MAP DESIGN

As aforementioned, the outer and inner 4-QAM constellation sequences, \mathbf{Y}_1 and \mathbf{Y}_2 , are superposed to form a 16-QAM constellation sequence $\mathbf{Y} = \sqrt{a} \cdot \mathbf{Y}_1 + \sqrt{1-a} \cdot \mathbf{Y}_2$ controlled by a power allocation coefficient a . Here, we set the total average transmit power to 1, and $a \in (0, 0.5)$. Then a and $1-a$ denote the power allocated to the outer and inner constellation sequences, respectively.

We illustrate in Fig. 7 the outer and inner 4-QAM constellation maps, as well as the resulted 16-QAM superposition constellation map. Since the inner constellation points do not carry valid information, the goal of both the legitimate user and the eavesdropper is to decode the outer constellation symbols.

Different power allocation coefficients result in distinct superposition constellation sequences, leading to varying SEPs when decoding the outer constellation symbols for two users. Different channel SNRs of the legitimate user and the eavesdropper also contribute to the difference in the SEP between the two users. Therefore, our objective is to analyze the SEP curves for both the legitimate user and the eavesdropper. We aim to identify the optimal a that maximizes the SEP of the eavesdropper while minimizing the SEP of the legitimate user. By doing so, we can prevent information leakage and achieve nearly information-theoretic security.

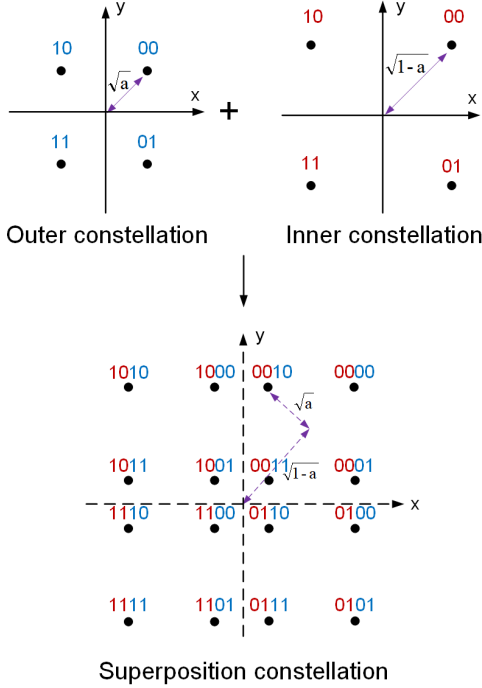


Fig. 7: 4-QAM + 4-QAM constellation with a power allocation coefficient a .

A. SEP Curves with respect to Power Allocation Coefficient

In this subsection, our goal is to derive the SEP of decoding the outer constellation points as a function of the power allocation coefficient a and the standard deviation of the AWGN σ for both users. We calculate the SEP by determining the symbol correct probability (SCP) of users when decoding the four outer constellation symbols. The maximum likelihood (ML) detector is employed to compute the SCP. It is essential to note that the noise follows a Gaussian distribution with a probability density function of $\mathcal{N}(x; 0, \sigma^2)$. Moreover, for any received constellation point, we assume that it is subjected to noise that is independent on the real and imaginary axes.

First, we analyze the case when the sent inner constellation symbol is '00'. Let us consider the example of decoding the outer constellation symbol '10', as illustrated in Fig. 8. The distance of the inner constellation points from the origin is $\sqrt{1-a}$, and the distance of the outer constellation points from the inner constellation points is \sqrt{a} , where $a \in (0, 0.5)$. Thus, we have $d_1 = \sqrt{a}/2$, $d_2 = \sqrt{(1-a)}/2$, and $d_2 > d_1$.

Let $SCP_{s_2}^{s_1}$ denote the probability that the received constellation point falls within the region s_2 , when the sent superposed symbol is s_1 . For example, SCP_{0010}^{0010} denotes the probability the received symbol falls within the upper right grey region in Fig. 8 when the sent symbol is 0010. We note that outer constellation symbol '10' can be successfully decoded as long as the received constellation points are within the four regions of '0010', '1010', '1110', and '0110'. Since the sent constellation symbol is '0010', we take its position as the origin of the maximum likelihood discrimination and calculate SCP_{0010}^{0010} , SCP_{1010}^{0010} , SCP_{0110}^{0010} and SCP_{1110}^{0010} .

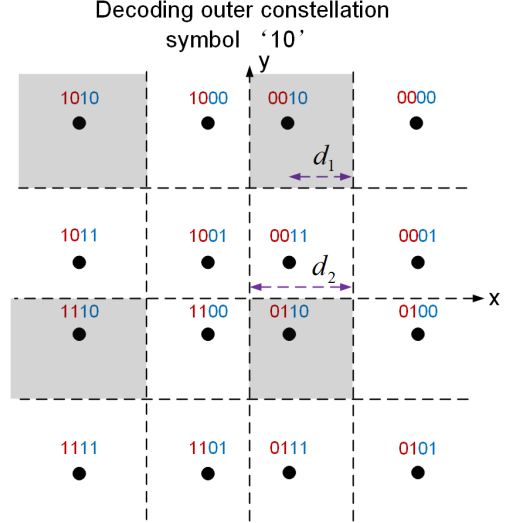


Fig. 8: Illustration of decoding the outer constellation symbol '10'.

We then have

$$SCP_{0010}^{0010} = \int_{-(d_2-d_1)}^{d_1} \int_{-d_1}^{\infty} f_{X,Y}(x, y) dx dy, \quad (13)$$

where $f_{X,Y}(x, y)$ is the joint probability density function of the Gaussian noise. Since the Gaussian noise on the real and imaginary axes in the constellation map is assumed to be independent of each other, $f_{X,Y}(x, y)$ is the product of the two marginal probability density functions, i.e., $f_{X,Y}(x, y) = f_X(x) \cdot f_Y(y) = \mathcal{N}(x; 0, \sigma^2) \cdot \mathcal{N}(y; 0, \sigma^2)$. This yields

$$\begin{aligned} SCP_{0010}^{0010} &= \int_{-(d_2-d_1)}^{d_1} N(x; 0, \sigma^2) dx \cdot \int_{-d_1}^{\infty} N(y; 0, \sigma^2) dy \\ &= \int_{-(d_2-d_1)}^{d_1} \frac{1}{\sqrt{2\pi}\sigma} \exp\left(-\frac{x^2}{2\sigma^2}\right) dx \cdot \\ &\quad \int_{-d_1}^{\infty} \frac{1}{\sqrt{2\pi}\sigma} \exp\left(-\frac{y^2}{2\sigma^2}\right) dy \\ &= \int_{-(d_2-d_1)}^{d_1} \frac{1}{\sqrt{2\pi}} \exp\left(-\frac{\left(\frac{x}{\sigma}\right)^2}{2}\right) d\left(\frac{x}{\sigma}\right) \cdot \\ &\quad \int_{-d_1}^{\infty} \frac{1}{\sqrt{2\pi}} \exp\left(-\frac{\left(\frac{y}{\sigma}\right)^2}{2}\right) d\left(\frac{y}{\sigma}\right) \\ &= \left[Q\left(\frac{-(d_2-d_1)}{\sigma}\right) - Q\left(\frac{d_1}{\sigma}\right) \right] \cdot Q\left(\frac{-d_1}{\sigma}\right), \end{aligned} \quad (14)$$

where $Q(x) = \frac{1}{\sqrt{2\pi}} \int_x^{\infty} \exp(-\frac{u^2}{2}) du$, and σ is the variance of channel noise.

We then calculate the probability of the received symbol in the '1010' region, i.e., the upper left grey region in Fig. 8,

when the sent symbol is '0010'. We have

$$\begin{aligned} SCP_{1010}^{0010} &= \int_{-\infty}^{-(2d_2-d_1)} N(x; 0, \sigma^2) dx \cdot \int_{-d_1}^{\infty} N(y; 0, \sigma^2) dy \\ &= Q\left(\frac{2d_2-d_1}{\sigma}\right) \cdot Q\left(\frac{-d_1}{\sigma}\right). \end{aligned} \quad (15)$$

Similarly, the SCP of decoding the constellation symbol '1110' and '0110' can be written as

$$\begin{aligned} SCP_{1110}^{0010} &= \int_{-\infty}^{-(2d_2-d_1)} N(x; 0, \sigma^2) dx \cdot \\ &\int_{-(2d_2+d_1)}^{-(d_1+d_2)} N(y; 0, \sigma^2) dy \\ &= Q\left(\frac{2d_2-d_1}{\sigma}\right) \cdot \left[Q\left(\frac{-(2d_2+d_1)}{\sigma}\right) - Q\left(\frac{-(d_1+d_2)}{\sigma}\right) \right]. \end{aligned} \quad (16)$$

$$\begin{aligned} SCP_{0110}^{0010} &= \int_{-(d_2-d_1)}^{d_1} N(x; 0, \sigma^2) dx \cdot \int_{-(2d_2+d_1)}^{-(d_1+d_2)} N(y; 0, \sigma^2) dy \\ &= \left[Q\left(\frac{-(d_2-d_1)}{\sigma}\right) - Q\left(\frac{d_1}{\sigma}\right) \right] \cdot \\ &\left[Q\left(\frac{-(2d_2+d_1)}{\sigma}\right) - Q\left(\frac{-(d_1+d_2)}{\sigma}\right) \right]. \end{aligned} \quad (17)$$

Therefore, the SCP of successfully decoding the outer constellation symbol '10' when the sent symbol is '0010', can be given as

$$SCP_{10}^{0010} = SCP_{0010}^{0010} + SCP_{1010}^{0010} + SCP_{1110}^{0010} + SCP_{0110}^{0010}. \quad (18)$$

Following the same process, we give the SCPs of successfully decoding the outer constellation symbols '00', '11', '01', when the sent symbols are '0000', '0011', '0001', respectively.

$$SCP_{00}^{0000} = SCP_{0000}^{0000} + SCP_{1000}^{0000} + SCP_{1100}^{0000} + SCP_{0100}^{0000}, \quad (19)$$

where

$$\begin{aligned} SCP_{0000}^{0000} &= Q\left(\frac{-d_1}{\sigma}\right)^2. \\ SCP_{1000}^{0000} &= \left[Q\left(\frac{-(2d_2+d_1)}{\sigma}\right) - Q\left(\frac{-(d_1+d_2)}{\sigma}\right) \right] \cdot Q\left(\frac{-d_1}{\sigma}\right). \\ SCP_{1100}^{0000} &= \left[Q\left(\frac{-(2d_2+d_1)}{\sigma}\right) - Q\left(\frac{-(d_1+d_2)}{\sigma}\right) \right]^2. \\ SCP_{0100}^{0000} &= \left[Q\left(\frac{-(2d_2+d_1)}{\sigma}\right) - Q\left(\frac{-(d_1+d_2)}{\sigma}\right) \right] \cdot Q\left(\frac{-d_1}{\sigma}\right). \end{aligned} \quad (20)$$

$$SCP_{11}^{0011} = SCP_{0011}^{0011} + SCP_{1011}^{0011} + SCP_{1111}^{0011} + SCP_{0111}^{0011}, \quad (21)$$

where

$$\begin{aligned} SCP_{0011}^{0011} &= \left[Q\left(\frac{-(d_2-d_1)}{\sigma}\right) - Q\left(\frac{d_1}{\sigma}\right) \right]^2. \\ SCP_{1011}^{0011} &= Q\left(\frac{2d_2-d_1}{\sigma}\right) \cdot \left[Q\left(\frac{-(d_2-d_1)}{\sigma}\right) - Q\left(\frac{d_1}{\sigma}\right) \right]. \\ SCP_{1111}^{0011} &= Q\left(\frac{2d_2-d_1}{\sigma}\right)^2. \\ SCP_{0111}^{0011} &= Q\left(\frac{2d_2-d_1}{\sigma}\right) \cdot \left[Q\left(\frac{-(d_2-d_1)}{\sigma}\right) - Q\left(\frac{d_1}{\sigma}\right) \right]. \end{aligned} \quad (22)$$

$$SCP_{01}^{0001} = SCP_{0001}^{0001} + SCP_{1001}^{0001} + SCP_{1101}^{0001} + SCP_{0101}^{0001}, \quad (23)$$

where

$$\begin{aligned} SCP_{0001}^{0001} &= Q\left(\frac{-d_1}{\sigma}\right) \cdot \left[Q\left(\frac{-(d_2-d_1)}{\sigma}\right) - Q\left(\frac{d_1}{\sigma}\right) \right]. \\ SCP_{1001}^{0001} &= \left[Q\left(\frac{-(2d_2+d_1)}{\sigma}\right) - Q\left(\frac{-(d_1+d_2)}{\sigma}\right) \right] \cdot \\ &\left[Q\left(\frac{-(d_2-d_1)}{\sigma}\right) - Q\left(\frac{d_1}{\sigma}\right) \right]. \\ SCP_{1101}^{0001} &= \left[Q\left(\frac{-(2d_2+d_1)}{\sigma}\right) - Q\left(\frac{-(d_1+d_2)}{\sigma}\right) \right] \cdot \\ &Q\left(\frac{2d_2-d_1}{\sigma}\right). \\ SCP_{0101}^{0001} &= Q\left(\frac{-d_1}{\sigma}\right) \cdot Q\left(\frac{2d_2-d_1}{\sigma}\right). \end{aligned} \quad (24)$$

As the simulation reveals, the probabilities of sending the four outer constellation points are approximately equal. Hence, when the sent inner constellation symbol is '00', the SEP of decoding the sent outer constellation symbols is

$$SEP^{00} = 1 - \frac{(SCP_{10}^{0010} + SCP_{00}^{0000} + SCP_{11}^{0011} + SCP_{01}^{0001})}{4}. \quad (25)$$

Subsequently, we compute the SEP of decoding the outer constellation symbols when the sent inner constellation symbols are '01', '10' and '11', respectively. Note that for different inner constellation symbols, the SCP of decoding the outer constellation symbols has certain symmetry. For example, the SCP of decoding the outer constellation symbol '00' when the sent inner constellation symbol is '01' is the same as the SCP of decoding the outer constellation symbol '10' when the sent inner constellation symbol is '00', i.e., $SCP_{00}^{0100} = SCP_{10}^{0010}$. This is equivalent to rotating the constellation map 90 degrees clockwise. It easily follows that the SEP of decoding the outer constellation symbols is the identical for all four sent inner constellation symbols, which can be written as

$$SEP^{00} = SEP^{01} = SEP^{10} = SEP^{11}. \quad (26)$$

Then we obtain the SEP of decoding the outer constellation symbols as shown in *Theorem 1*.

Theorem 1: According to equations (13)-(26), when $M = 2$ and the superposition constellation sequence is M^2 -QAM

constellation sequence, the formula for SEP of decoding the outer M -QAM constellation symbols can be written as

$$SEP = \frac{(SEP^{00} + SEP^{01} + SEP^{10} + SEP^{11})}{4} = SEP^{00}, \quad (27)$$

where SEP^{00} is given in (25).

Recall that the channel SNR of the legitimate user and the eavesdropper is denoted by SNR_{leg} and SNR_{eve} , respectively. We plot the curves of the SEP by the legitimate user and the eavesdropper with regards to the power allocation coefficient a in Fig. 9, when $SNR_{leg} = 20\text{dB}$ and $SNR_{eve} = -10\text{dB}$. We

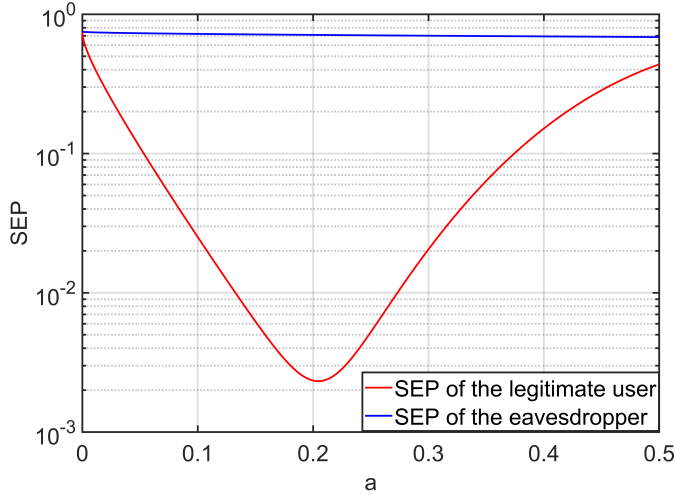


Fig. 9: The SEP of the legitimate user and the eavesdropper when $SNR_{leg} = 20\text{dB}$ and $SNR_{eve} = -10\text{dB}$.

can observe that the SEP of the eavesdropper remains high and decreases very slowly with a since the eavesdropper suffers from poor channel. It can also be observed that the SEP of the legitimate user initially decreases rapidly and then increases rapidly. Based on this finding, we select a power allocation coefficient a such that the SEP of the legitimate user is relatively low, while the SEP of the eavesdropper is high enough. This can prevent information leakage to the eavesdropper and makes it less likely for them to recover useful information. For example, in Fig. 9, when we choose $a = 0.055$, the SEP of the eavesdropper is 73%, making it almost impossible to recover any valid information. Meanwhile, the SEP of the legitimate user is only 9.4%, ensuring the performance of the legitimate user.

Based on the above SEP results, to find the optimal power allocation coefficient a under a certain legitimate user-eavesdropper SNR pair, we formulate an optimization algorithm as follows

$$\min SEP_{leg} \text{ s.t. } SEP_{eve} \geq b, \quad (28)$$

where SEP_{leg} and SEP_{eve} are the SEP of the legitimate user and the eavesdropper, respectively, and b is the given constraint on SEP_{eve} , limiting information leakage to the eavesdropper. A higher value of b indicates a more secure system, but it comes at the cost of performance loss for the legitimate user. Based on the proposed optimization algorithm, we give the

optimal value of a under different legitimate user-eavesdropper SNR pairs and different values of b , as shown in Table. I.

Legitimate user SNR (dB)	Eavesdropper SNR (dB)	b (%)	a
20	-15	74	0.040
		73	0.158
		72	0.347
	-10	71	-
		74	0.014
		73	0.055
		72	0.121
	-5	71	0.209
		74	0.006
		73	0.025
	0	72	0.051
		71	0.087
74		0.003	
5	73	0.014	
	72	0.030	
	71	0.052	
	74	0.001	
	73	0.004	
	72	0.009	
	71	0.017	

TABLE I: The optimal value of a under different legitimate user-eavesdropper SNR pairs and different values of b .

B. Equivalent Channel Capacity

In this subsection, we analyze the gap between the channel capacity of the proposed superposition code based transmission scheme and the wiretap channel capacity. Note that the channel capacity is determined by channel SNR according to the Shannon equation. Hence, equivalently, we compare the actual equivalent channel SNR based on different thresholds b with the wiretap channel capacity equivalent SNR to evaluate the channel capacity gap.

We denote the wiretap channel capacity equivalent SNR as SNR_{equ}^1 . We can calculate the wiretap channel capacity $C_{wiretap}$ [26] by

$$C_{wiretap} = \max\{B \log_2(1+SNR_{leg}) - B \log_2(1+SNR_{eve}), 0\}, \quad (29)$$

where B is the channel bandwidth. We recall that SNR_{leg} and SNR_{eve} is the the channel SNR of the legitimate user and the eavesdropper, respectively. We then have

$$B \log_2(1+SNR_{equ}^1) = B \log_2(1+SNR_{leg}) - B \log_2(1+SNR_{eve}), \quad (30)$$

which yields

$$\begin{aligned} SNR_{equ}^1 &= 2^{(\log_2(1+SNR_{leg}) - \log_2(1+SNR_{eve}))} - 1 \\ &= 10 \log_{10}(2^{(\log_2(1+SNR_{leg}) - \log_2(1+SNR_{eve}))} - 1) \text{ (dB)}. \end{aligned} \quad (31)$$

Different thresholds b correspond to different optimal power allocation coefficients $a = g(b)$ by solving the optimization problem in (28). We denote the actual equivalent channel SNR for a given threshold b by $SNR_{equ}^2(b)$, which can be calculated by

$$SNR_{equ}^2(b) = 10 \log_{10} \left(\frac{g(b)P}{\sigma_1^2} \right) \text{ (dB)}. \quad (32)$$

We assess the capacity loss for security by comparing the actual equivalent channel SNR $SNR_{equ}^2(b)$ with the wiretap

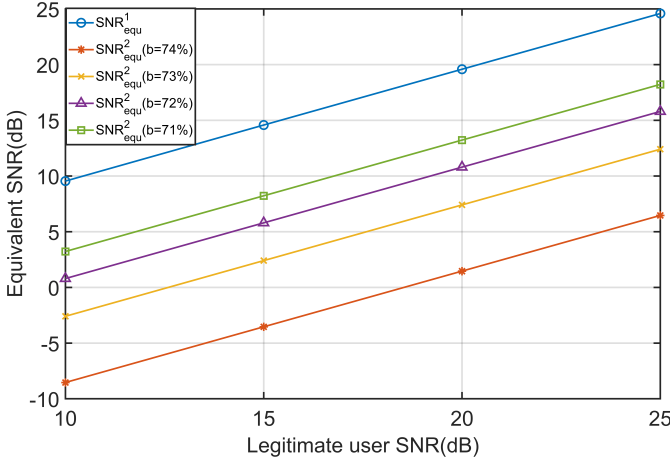


Fig. 10: Equivalent channel SNR curves under different SNR_{leg} values when $\text{SNR}_{\text{eve}} = -10\text{dB}$.

channel capacity equivalent SNR $\text{SNR}_{\text{equ}}^1$, as illustrated in Fig. 10. We can observe that the gap between the actual equivalent channel SNR and the wiretap channel capacity equivalent SNR becomes smaller as the threshold b decreases. It is important to note that the wiretap channel capacity represents a scenario without security considerations. As the threshold b increases, our system sacrifices more channel capacity for enhanced security. Conversely, with a lower threshold b , the channel capacity of our system increases, but the security level decreases. This highlights the inherent trade-off between the security and channel capacity of our system.

V. SIMULATION RESULTS

A. Experimental Settings

1) *Dataset*: Our experiments utilize the CIFAR-10 dataset [39], comprising 50,000 training images and 10,000 testing images. All the images in the dataset are 32×32 RGB images.

2) *Compression Ratio*: We denote the number of symbols in the source image by n and the number of symbols transmitted over the channel by k . The compression ratio is denoted as $CR = k/n$. In this paper, the compression ratio falls within the set $CR \in \{1/24, 2/24, 3/24, 4/24, 5/24, 6/24, 12/24\}$.

3) *Training Settings*: The batch size is configured as 512, and training employs the Adam optimizer [40]. During the initial training stage, we train the legitimate semantic encoder-decoder pair. The learning rate schedule is as follows: 2×10^{-4} for 30 epochs, 1×10^{-4} for 40 epochs, 5×10^{-5} for 40 epochs, and 1×10^{-5} for the remaining 40 epochs. It's noteworthy that the learning rate of the 4-QAM modulator is half of the specified learning rate. In the subsequent training stage, only the semantic decoder of the eavesdropper is trained, with the learning rate following this sequence: 2×10^{-4} for 50 epochs, 5×10^{-5} for 50 epochs, and 1×10^{-5} for the final 50 epochs.

4) *Performance Metric*: We utilize the peak signal-to-noise ratio (PSNR) as a metric to evaluate the image recovery quality of the users. PSNR is defined by the formula:

$$\text{PSNR}(\mathbf{X}, \hat{\mathbf{X}}) = 10 \log_{10} \left(\frac{\text{MAX}^2}{\text{MSE}(\mathbf{X}, \hat{\mathbf{X}})} \right) \text{ (dB)}. \quad (33)$$

Here, MAX represents the maximum pixel value within the source image, which is 255 for a 24-bit RGB image. The MSE is calculated as:

$$\text{MSE}(\mathbf{X}, \hat{\mathbf{X}}) = \|\mathbf{X} - \hat{\mathbf{X}}\|_2^2. \quad (34)$$

5) *The Benchmarks*: We utilize three benchmarks for comparison purposes. In the first benchmark, Alice transmits a 16-QAM constellation sequence \mathbf{Y}_1 directly to the legitimate user without employing a superposition code. In this scenario, there is no randomly generated constellation sequence \mathbf{Y}_2 , and no power allocation coefficient a is needed. This benchmark essentially represents a digital SeCom system without specific security design considerations. All other parameters and settings align with the proposed system. We refer to this benchmark as *16-QAM without Superposition*.

In the second benchmark, we implement the adversarial training method proposed in [20]. Following the network structure outlined in [20], we consider an analog SeCom system without modulation and superposition code. The semantic encoder generates the channel input symbols, which are directly fed into the AWGN channel. In this benchmark, the structure of the legitimate semantic encoder-decoder pair is replaced with the network structure proposed in [7]. For this benchmark, we adopt a two-stage training strategy. In the first training stage, an adversarial training strategy is employed, involving a minimax game between the Alice and Bob pair and Eve. Both the legitimate semantic encoder-decoder pair and the semantic decoder of the eavesdropper are trained. The loss function of the first stage is expressed as:

$$\mathcal{L}_{\text{benchmark}}^1 = \text{MSE}(\mathbf{X}, \hat{\mathbf{X}}_1) - \lambda \cdot \text{MSE}(\mathbf{X}, \hat{\mathbf{X}}_2), \quad (35)$$

where $\lambda = 2 \times 10^{-2}$ is a trade-off hyperparameter. The legitimate network aims to minimize $\mathcal{L}_{\text{benchmark}}^1$, while the eavesdropper's network (the semantic decoder of the eavesdropper) aims to maximize it. The training follows the approach of generative adversarial networks (GANs), with iterative parameter updates for both networks. After one training step of the legitimate network, the eavesdropper's network is trained for one step. Subsequently, in the second training stage, only the eavesdropper's network is trained to enhance its performance. The loss function of the second stage is given by:

$$\mathcal{L}_{\text{benchmark}}^2 = \text{MSE}(\mathbf{X}, \hat{\mathbf{X}}_2). \quad (36)$$

All other settings remain consistent with the proposed system, and we refer to this benchmark as *Adversarial Training*.

In the third benchmark, both the inner and outer 4-QAM constellation sequences \mathbf{Y}_1 and \mathbf{Y}_2 are randomly generated. They are subsequently superposed to generate 16-QAM superposition constellation sequence. This benchmark is used to examine the PSNR performance when the signal received by the eavesdropper is a random constellation sequence to analyze whether our proposed system can achieve information-theoretic security. The other settings remain consistent with the proposed system. We name this benchmark as *Random constellation sequence*.

B. The Performance Comparison on Security of Different Approaches

In this subsection, we assess the security of our proposed secure digital SeCom system in comparison to benchmarks. Specifically, we examine the PSNR performance of the eavesdropper, where a lower PSNR indicates a more secure system. Fig. 11 illustrates the PSNR performance of the eavesdropper across different methods and compression ratios. The channel conditions are configured with $\text{SNR}_{\text{leg}} = 20\text{dB}$ and $\text{SNR}_{\text{eve}} = -10\text{dB}$. In our proposed system, we set the eavesdropper's Symbol Error Probability (SEP) to be 74%, corresponding to $b = 74\%$ and, consequently, the power allocation coefficient $a = 0.014$.

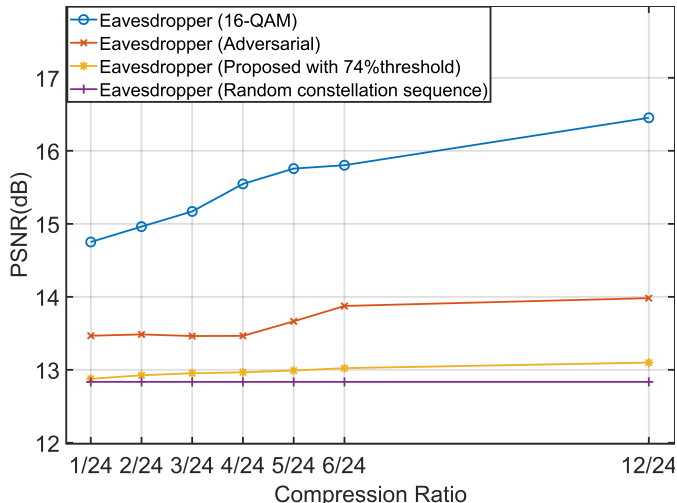


Fig. 11: The PSNR performance of the eavesdropper by different approaches. Here, $\text{SNR}_{\text{leg}} = 20\text{dB}$ and $\text{SNR}_{\text{eve}} = -10\text{dB}$.

From Fig. 11, it is evident that the security of our proposed system surpasses both *16-QAM without Superposition* and *Adversarial Training*. *16-QAM without Superposition*, lacking specific security guarantee, serves as a baseline to gauge the minimum security, highlighting the improvement achieved by other methods. The numerical results reveal two main security disadvantages in *16-QAM without Superposition*. Firstly, the only obstacle for the eavesdropper to obtain semantic information is the high-power AWGN and the low compression ratio. This is not sufficient to prevent the eavesdropper from reconstructing the original image data with a relatively high PSNR. For instance, at a compression ratio of 12/24, the PSNR of the recovered image can reach 16.45dB, surpassing *Adversarial Training* by 2.47dB and our proposed system by 3.35dB. Secondly, information leakage increases rapidly with the growth of the compression ratio, rendering the security of the SeCom system extremely vulnerable in the high compression rate regime. For instance, at a compression ratio of 12/24, the PSNR of the reconstructed image rises to 16.45dB, which is 1.7dB higher than when the compression ratio is 1/24. These findings underscore the importance of designing secure SeCom systems.

The security enhancement of *Adversarial Training* is notable compared to *16-QAM without Superposition*. This improvement is attributed to the strategic engagement between the legitimate user and the eavesdropper, allowing the former to minimize information leakage actively. Consequently, there is a significant reduction in the PSNR performance of the eavesdropper compared to *16-QAM without Superposition*. For instance, at a compression ratio of 1/24, *Adversarial Training* lowers the PSNR performance of the eavesdropper by 1.28dB, and at a compression ratio of 12/24, it reduces the PSNR performance by 2.47dB. This demonstrates the impact of actively defending against the eavesdropper in improving SeCom system security. However, it's worth noting that the security of *Adversarial Training* diminishes notably at high compression ratios. For instance, there is a 0.4-0.5dB improvement in the PSNR performance of the eavesdropper as the compression rate surpasses 4/24. This implies that, while *Adversarial Training* proves effective at low compression rates, its ability to achieve information-theoretic security diminishes at relatively high compression rates due to increased information leakage.

In contrast, our proposed system exhibits superior security. For instance, in our system, the PSNR performance of the eavesdropper is reduced by 0.6-0.9dB compared to *Adversarial Training*. Furthermore, with an increase in compression rate from 1/24 to 12/24, the PSNR performance of the eavesdropper improves by only 0.2dB. It's essential to highlight that the PSNR performance of the eavesdropper in our proposed system is approximately 12.9-13.1dB, which is nearly equivalent to the scenario where the eavesdropper receives a random constellation sequence. This suggests that the eavesdropper is not able to recover much of the valid information from the received signals, which proves the information-theoretic security of the proposed approach.

In Fig. 12, we visually compare the reconstructed images at the eavesdropper by the proposed system and the benchmarks. Fig. 12(a) is the source image \mathbf{X} , Fig. 12(b), Fig. 12(c) and Fig. 12(d) show the recovered images by the eavesdropper in our proposed system, *16-QAM without Superposition*, and *Adversarial Training*, respectively. Comparing the recovered images of the eavesdropper, we demonstrate that the security of our proposed system is better than the two benchmarks. The source image, in this case, is a picture of a dog. In the *16-QAM without Superposition* benchmark, the eavesdropper can recover a clear outline of the source image. In *Adversarial Training*, the eavesdropper can only recover some blurred background. However, in our proposed system, the recovered image of the eavesdropper is nearly completely black, making it extremely challenging for the eavesdropper to obtain any meaningful information. Therefore, our proposed system excels over the benchmarks in preventing information leakage to the eavesdropper.

C. Performance under Different SEPs of the Eavesdropper

In this subsection, we evaluate the performance and security of the proposed system under different SEP thresholds, aiming to analyze the impact of thresholds on both aspects.

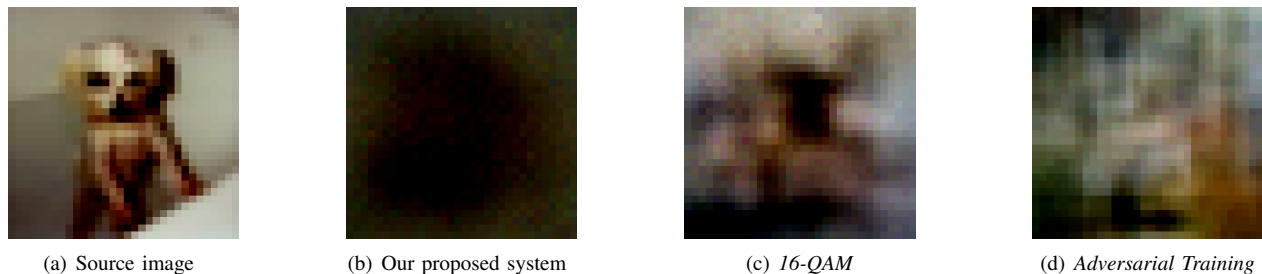


Fig. 12: Visual analysis of the reconstructed images at the eavesdropper. The channel conditions are set at $\text{SNR}_{\text{leg}} = 20\text{dB}$ and $\text{SNR}_{\text{eve}} = -10\text{dB}$. The compression ratio is 6/24.

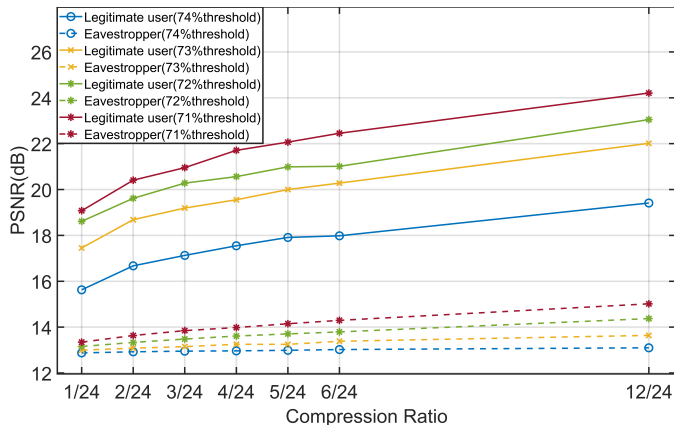


Fig. 13: PSNR performance under different SEPs of the eavesdropper, i.e., different thresholds b . Here, $\text{SNR}_{\text{leg}} = 20\text{dB}$ and $\text{SNR}_{\text{eve}} = -10\text{dB}$.

Specifically, we evaluate the PSNR performance of both the legitimate user and the eavesdropper, as illustrated in Fig. 13. The channel conditions are configured with $\text{SNR}_{\text{leg}} = 20\text{dB}$ and $\text{SNR}_{\text{eve}} = -10\text{dB}$. The thresholds vary from 71% to 74% in 1% increments, where a lower threshold b corresponds to a larger power allocation coefficient a . To represent the PSNR performance at the same threshold, consistent color curves are used. The solid line depicts the PSNR performance of the legitimate user, while the dashed line represents the PSNR performance of the eavesdropper.

From Fig. 13, it is evident that a lower threshold leads to better PSNR performance for both the legitimate user and the eavesdropper. This is because, as the SEP of the eavesdropper decreases, the SEP of the legitimate user also decreases. Specifically, the system with a 71% threshold exhibits the best PSNR performance for the legitimate user but has the weakest security, as the PSNR performance of the eavesdropper is relatively high at this point. As the threshold increases, the PSNR performance of the legitimate user decreases while its security improves. The system with a 74% threshold demonstrates the highest security, making it nearly impossible for the eavesdropper to recover any useful information. In our proposed system, the PSNR performance of the eavesdropper improves gradually as the compression ratio increases. For the system with a 71% threshold, as the compression ratio increases from 1/24 to 12/24, the PSNR performance of

the eavesdropper improves by 1.7dB. In contrast, for the system with a 74% threshold, the PSNR performance of the eavesdropper improves by only 0.2dB. Therefore, to achieve high security, a threshold of 74% should be employed to minimize information leakage. However, if high security is not a strict requirement, the threshold can be appropriately lowered to enhance the PSNR performance of the legitimate user.

We also present the images reconstructed by the legitimate user and the eavesdropper at various thresholds, as illustrated in Fig.14 and Fig.15, respectively. In Fig.14, it is observed that the reconstructed image by the legitimate user becomes more distinct as the threshold decreases. Fig.14(a) only provides a basic outline of the source image, while Fig.14(d) manages to capture more details of the source image. On the other hand, Fig.15 reveals that even with a lowered threshold, the reconstructed image by the eavesdropper contains minimal useful information and remains largely blurred.

D. Performance of Our Proposed System under Different Legitimate user-Eavesdropper SNR Pairs

In this subsection, we assess the performance of the proposed system across diverse channel conditions, as illustrated in Fig. 16, where the channel conditions are set at $\text{SNR}_{\text{leg}} = 20\text{dB}$ and $\text{SNR}_{\text{eve}} \in \{-15, -10, -5, 0, 5\}\text{dB}$. With a fixed threshold b , we observe that the SEP of the legitimate user decreases as the difference between the legitimate channel SNR SNR_{leg} and the eavesdropper channel SNR SNR_{eve} increases. We can observe that with SNR_{leg} at 20dB and the threshold b at 74%, the PSNR performance of the legitimate user decreases with the eavesdropper channel SNR SNR_{eve} . Conversely, the PSNR performance of the eavesdropper shows only marginal improvement. Even with an elevation in the eavesdropper channel SNR SNR_{eve} from -15dB to 5dB, the improvement in the PSNR performance of the eavesdropper ranges from 0.1 to 0.7dB. Moreover, as the compression rate increases, there is also slight enhancement in the PSNR performance of the eavesdropper. These findings indicate that even with improvements in the eavesdropper's channel conditions or an increase in the number of acquired symbols, our proposed system ensures that the eavesdropper is nearly incapable of recovering the source image, thereby achieving near-information-theoretic security. We infer that further increases in SNR_{eve} (e.g., to 10dB or higher) may still compromise

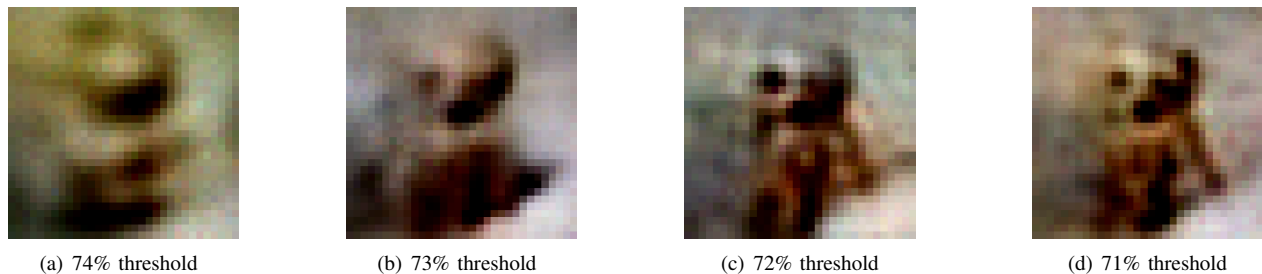


Fig. 14: Visual analysis of the reconstructed images by the legitimate user under different thresholds b . The channel conditions are set at $\text{SNR}_{\text{leg}} = 20\text{dB}$ and $\text{SNR}_{\text{eve}} = -10\text{dB}$. The compression ratio is $12/24$.

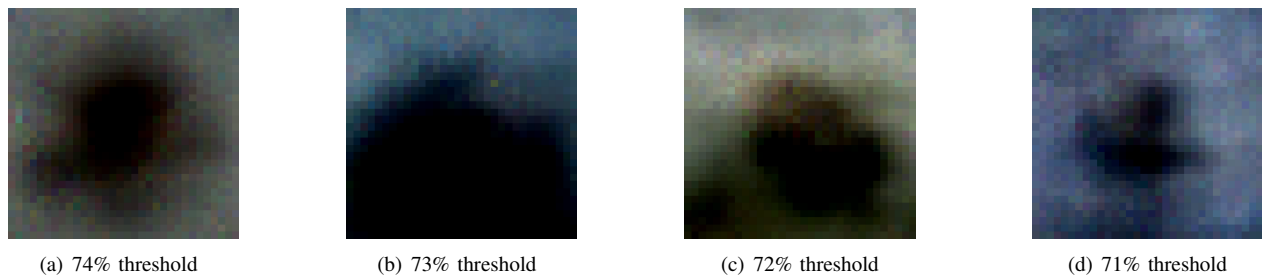


Fig. 15: Visual analysis of the reconstructed images by the eavesdropper under different thresholds b . The channel conditions are set at $\text{SNR}_{\text{leg}} = 20\text{dB}$ and $\text{SNR}_{\text{eve}} = -10\text{dB}$. The compression ratio is $12/24$.

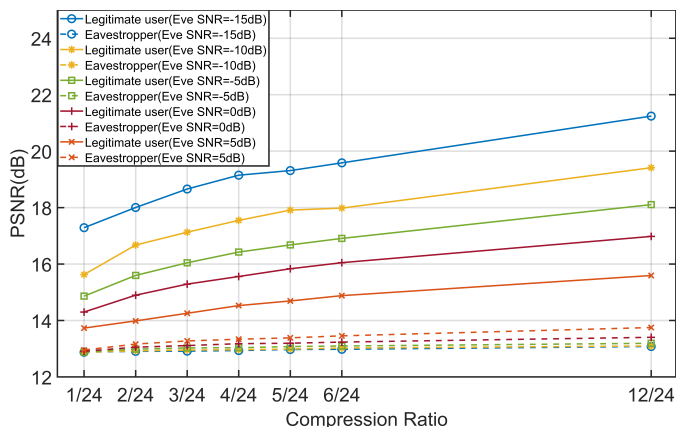


Fig. 16: PSNR performance under different legitimate user-eavesdropper SNR pairs. Here the threshold b is set to 74% and $\text{SNR}_{\text{leg}} = 20\text{dB}$.

system security, even with a 74% threshold, suggesting the need for a higher threshold. Conversely, when SNR_{eve} is low (e.g., -15dB) and the compression rate is low (e.g., $1/24$), good security can be achieved even with a threshold value of 71%. This validates the system's adaptability to different application scenarios, allowing us to tailor thresholds for optimal performance and near-information-theoretic security under various channel conditions.

VI. CONCLUSION

In this paper, we introduced a secure digital SeCom system based on superposition codes for wiretap channels. The proposed method involves generating a two-layered discrete

superposition code through the overlay of one 4-QAM modulation constellation map onto another. Semantic information is modulated onto the outer constellation map, and a random constellation point is uniformly selected within the inner constellation. The power allocation between the inner and outer constellation maps is adjusted to achieve a high Symbol Error Probability (SEP) for the eavesdropper, ensuring security, while maintaining a low SEP for the legitimate user to facilitate data transmission. This method offers two significant advantages over conventional approaches. Firstly, it enables nearly information-theoretically secure data transmission by adjusting power allocation and setting the eavesdropper's SEP to a required level. At a SEP that is high enough, the eavesdropper essentially decodes the outer constellation point as poorly as blinded random guessing. Secondly, the security performance of the proposed method remains robust even as the compression rate increases. This implies that we can enhance the legitimate user's performance by transmitting more data without concerns about information leakage. These advantages position our proposed method as a practical and secure SeCom solution, particularly suitable for scenarios with ample communication resources but stringent security requirements.

Looking ahead, our future efforts will focus on further improving the performance of the legitimate user. We believe that by encoding the inner constellation points with a random codeword from a codebook known only to the transmitter and legitimate user, rather than a totally random symbol sequence, the legitimate user can decode the energy jamming signal carried on the inner constellation points. This enhancement is expected to result in better performance in decoding the outer constellation points, further strengthening the security

and efficacy of our proposed method.

REFERENCES

- [1] Z. Qin, X. Tao, J. Lu, W. Tong, and G. Y. Li, "Semantic communications: Principles and challenges," *arXiv preprint arXiv:2201.01389*, 2021.
- [2] J. Liu, S. Shao, W. Zhang, and H. V. Poor, "An indirect rate-distortion characterization for semantic sources: General model and the case of gaussian observation," *IEEE Transactions on Communications*, vol. 70, no. 9, pp. 5946–5959, 2022.
- [3] D. Gündüz, Z. Qin, I. E. Aguerri, H. S. Dhillon, Z. Yang, A. Yener, K. K. Wong, and C.-B. Chae, "Beyond transmitting bits: Context, semantics, and task-learning for natural language communications," *IEEE Journal on Selected Areas in Communications*, vol. 41, no. 1, pp. 5–41, 2022.
- [4] Y. LeCun, Y. Bengio, and G. Hinton, "Deep learning," *nature*, vol. 521, no. 7553, pp. 436–444, 2015.
- [5] K. He, X. Zhang, S. Ren, and J. Sun, "Deep residual learning for image recognition," in *Proceedings of the IEEE conference on computer vision and pattern recognition*, 2016, pp. 770–778.
- [6] D. W. Otter, J. R. Medina, and J. K. Kalita, "A survey of the usages of deep learning for natural language processing," *IEEE transactions on neural networks and learning systems*, vol. 32, no. 2, pp. 604–624, 2020.
- [7] E. Boursoulatte, D. B. Kurka, and D. Gündüz, "Deep joint source-channel coding for wireless image transmission," *IEEE Transactions on Cognitive Communications and Networking*, vol. 5, no. 3, pp. 567–579, 2019.
- [8] N. Farsad, M. Rao, and A. Goldsmith, "Deep learning for joint source-channel coding of text," in *2018 IEEE international conference on acoustics, speech and signal processing (ICASSP)*. IEEE, 2018, pp. 2326–2330.
- [9] T. Han, Q. Yang, Z. Shi, S. He, and Z. Zhang, "Semantic-aware speech to text transmission with redundancy removal," in *2022 IEEE International Conference on Communications Workshops (ICC Workshops)*. IEEE, 2022, pp. 717–722.
- [10] T. Han, Q. Yang, Z. Shi, S. He, and Z. Zhang, "Semantic-preserved communication system for highly efficient speech transmission," *IEEE Journal on Selected Areas in Communications*, vol. 41, no. 1, pp. 245–259, 2022.
- [11] Z. Weng, Z. Qin, X. Tao, C. Pan, G. Liu, and G. Y. Li, "Deep learning enabled semantic communications with speech recognition and synthesis," *IEEE Transactions on Wireless Communications*, 2023.
- [12] C.-H. Lee, J.-W. Lin, P.-H. Chen, and Y.-C. Chang, "Deep learning-constructed joint transmission-recognition for internet of things," *IEEE Access*, vol. 7, pp. 76 547–76 561, 2019.
- [13] M. Jankowski, D. Gündüz, and K. Mikołajczyk, "Wireless image retrieval at the edge," *IEEE Journal on Selected Areas in Communications*, vol. 39, no. 1, pp. 89–100, 2020.
- [14] Z. Zhang, Q. Yang, S. He, and Z. Shi, "Semantic communication approach for multi-task image transmission," in *2022 IEEE 96th Vehicular Technology Conference (VTC2022-Fall)*. IEEE, 2022, pp. 1–2.
- [15] P. Jiang, C.-K. Wen, S. Jin, and G. Y. Li, "Wireless semantic communications for video conferencing," *IEEE Journal on Selected Areas in Communications*, vol. 41, no. 1, pp. 230–244, 2022.
- [16] H. Xie, Z. Qin, X. Tao, and K. B. Letaief, "Task-oriented multi-user semantic communications," *IEEE Journal on Selected Areas in Communications*, vol. 40, no. 9, pp. 2584–2597, 2022.
- [17] M. Shen, J. Wang, H. Du, D. Niyato, X. Tang, J. Kang, Y. Ding, and L. Zhu, "Secure semantic communications: Challenges, approaches, and opportunities," *IEEE Network*, 2023.
- [18] Y. Chen, Q. Yang, Z. Shi, and J. Chen, "The model inversion eavesdropping attack in semantic communication systems," *arXiv preprint arXiv:2308.04304*, 2023.
- [19] E. Erdemir, P. L. Dragotti, and D. Gündüz, "Privacy-aware communication over a wiretap channel with generative networks," in *ICASSP 2022-2022 IEEE International Conference on Acoustics, Speech and Signal Processing (ICASSP)*. IEEE, 2022, pp. 2989–2993.
- [20] T. Marchioro, N. Laurenti, and D. Gündüz, "Adversarial networks for secure wireless communications," in *ICASSP 2020-2020 IEEE International Conference on Acoustics, Speech and Signal Processing (ICASSP)*. IEEE, 2020, pp. 8748–8752.
- [21] T.-Y. Tung and D. Gündüz, "Deep joint source-channel and encryption coding: Secure semantic communications," in *ICC 2023-IEEE International Conference on Communications*. IEEE, 2023, pp. 5620–5625.
- [22] R. Lindner and C. Peikert, "Better key sizes (and attacks) for lwe-based encryption," in *Topics in Cryptology—CT-RSA 2011: The Cryptographers' Track at the RSA Conference 2011, San Francisco, CA, USA, February 14-18, 2011. Proceedings*. Springer, 2011, pp. 319–339.
- [23] W. Buchanan and A. Woodward, "Will quantum computers be the end of public key encryption?" *Journal of Cyber Security Technology*, vol. 1, no. 1, pp. 1–22, 2017.
- [24] S. Y. Yan, *Quantum attacks on public-key cryptosystems*. Springer, 2013, vol. 207.
- [25] E. Biham, "New types of cryptanalytic attacks using related keys," *Journal of Cryptology*, vol. 7, pp. 229–246, 1994.
- [26] A. D. Wyner, "The wire-tap channel," *Bell system technical journal*, vol. 54, no. 8, pp. 1355–1387, 1975.
- [27] H. Tyagi and A. Vardy, "Explicit capacity-achieving coding scheme for the gaussian wiretap channel," in *2014 IEEE International Symposium on Information Theory*. IEEE, 2014, pp. 956–960.
- [28] Y. Bo, Y. Duan, S. Shao, and M. Tao, "Learning based joint coding-modulation for digital semantic communication systems," in *2022 14th International Conference on Wireless Communications and Signal Processing (WCSP)*. IEEE, 2022, pp. 1–6.
- [29] Y. E. Sagduyu, T. Erpek, S. Ulukus, and A. Yener, "Is semantic communications secure? a tale of multi-domain adversarial attacks," *arXiv preprint arXiv:2212.10438*, 2022.
- [30] H. Du, J. Wang, D. Niyato, J. Kang, Z. Xiong, M. Guizani, and D. I. Kim, "Rethinking wireless communication security in semantic internet of things," *IEEE Wireless Communications*, vol. 30, no. 3, pp. 36–43, 2023.
- [31] Y. Lin, H. Du, D. Niyato, J. Nie, J. Zhang, Y. Cheng, and Z. Yang, "Blockchain-aided secure semantic communication for ai-generated content in metaverse," *IEEE Open Journal of the Computer Society*, vol. 4, pp. 72–83, 2023.
- [32] Z. Yang, M. Chen, G. Li, Y. Yang, and Z. Zhang, "Secure semantic communications: Fundamentals and challenges," *arXiv preprint arXiv:2301.01421*, 2023.
- [33] X. Luo, Z. Chen, M. Tao, and F. Yang, "Encrypted semantic communication using adversarial training for privacy preserving," *IEEE Communications Letters*, 2023.
- [34] L. Zhao, D. Wu, and L. Zhou, "Data utilization versus privacy protection in semantic communications," *IEEE Wireless Communications*, vol. 30, no. 3, pp. 44–50, 2023.
- [35] Y. Wang, W. Yang, P. Guan, Y. Zhao, and Z. Xiong, "Star-ris-assisted privacy protection in semantic communication system," *arXiv preprint arXiv:2306.12675*, 2023.
- [36] Y. Wang, S. Guo, Y. Deng, H. Zhang, and Y. Fang, "Privacy-preserving task-oriented semantic communications against model inversion attacks," *arXiv preprint arXiv:2312.03252*, 2023.
- [37] E. C. Cejudo, H. Zhu, and O. Alluhaibi, "On the power allocation and constellation selection in downlink noma," in *2017 IEEE 86th Vehicular Technology Conference (VTC-Fall)*. IEEE, 2017, pp. 1–5.
- [38] E. Jang, S. Gu, and B. Poole, "Categorical reparameterization with gumbel-softmax," *arXiv preprint arXiv:1611.01144*, 2016.
- [39] A. Krizhevsky, G. Hinton *et al.*, "Learning multiple layers of features from tiny images," 2009.
- [40] D. P. Kingma and J. Ba, "Adam: A method for stochastic optimization," *arXiv preprint arXiv:1412.6980*, 2014.